



Experimental analysis of foulant deposition in submerged hollow fiber membrane modules

Yoon-Jin Kim, Taekgun Yun, Jinsik Sohn, Sangho Lee*

School of Civil and Environmental Engineering, Kookmin University, Jeongneung-Dong, Seongbuk-Gu, Seoul 136-702, Republic of Korea

Tel. +82 2 910 4529; Fax: +82 2 910 4939; email: sanghlee@kookmin.ac.kr

Received 28 October 2012; Accepted 28 December 2012

ABSTRACT

Hollow fiber ultrafiltration (UF) membranes have been widely employed for water treatment and pretreatment for seawater desalination. Nevertheless, there are challenges in design and optimization of hollow fiber modules because their efficiency depends on their geometric factors and filtration conditions. In this work, we focused on the analysis of submerged UF membranes for better understanding the correlation between hydrodynamic conditions and fouling phenomena. The local flux profiles were calculated based on the Hagen–Poiseuille equation. The results were compared with the experimental results of local fouling patterns, which were obtained based on an image analysis technique using a blue indigo solution. The experimental and theoretical results agreed qualitatively. The results in this study suggest that the methods demonstrated in this study can provide in-depth information such as local flux and pressure profiles, local foulant deposition, and the effect of fiber geometry and operation conditions.

Keywords: Submerged hollow fiber membrane; Pretreatment; Ultrafiltration; Module; Fiber length; Local fouling; Image analysis

1. Introduction

Membrane processes such as microfiltration (MF) or ultrafiltration (UF) have been widely employed in various applications [1–3]. The use of MF and UF has been studied by researches since the mid-1990s and cost reduction in these technologies in the mid-2000s led to the installation of MF/UF in water treatment and seawater desalination plants [4,5]. Moreover,

membrane bioreactors have recently emerged as an important technology for water reuse due to its capability of trans-forming wastewater to high quality effluent suitable for many applications [5]. Of particular interest in practical implementation are hollow fiber MF/UF modules, because they have many advantages such as high specific membrane area, relative low cost production, and easy operation [6–8]. Although submerged membranes are primarily used for membrane bioreactor, they also have potential for the treatment of drinking water and feed water to seawater reverse osmosis [9–12].

*Corresponding author.

However application of hollow fiber MF and UF modules is often limited by membrane fouling. The membranes are susceptible to fouling by suspended solids, colloidal matters, and organics in the feed stream. In addition, there is an internal pressure drop caused by flowing medium in the fiber, leading to a decrease in trans-membrane pressure (TMP) along the fiber. Accordingly, local fluxes are not uniform over the membrane, which also results in problems such as local fouling phenomena, increased energy consumption, and deterioration of overall membrane performance.

This study intended to analyze the efficiency of hollow fiber UF membranes for better understanding the dependence of fouling on their hydrodynamic conditions. The local pressure and flux profiles were calculated based on the Hagen–Poiseuille equation. An experimental method using blue Indigo particles was applied to measure local fouling rate in laboratory-scale hollow fiber membranes. The originality of the paper lies in the demonstration of experimental technique for visualizing foulant deposition together with the theoretical analysis of local flux distribution. The results from theoretical calculation and experimental measurement were compared to understand hydrodynamic characteristic of hollow fiber UF modules.

2. Theory

We have applied the hydrodynamic model equations for pressure drop outside and inside hollow fibers to predict the performance of dead-end UF over a wide range of conditions. We only give a broad outline of the model here, since details are provided

separately. Fig. 1 shows the flow and geometry in a hollow fiber UF membrane. The permeate flows inside the fibers. The permeate outlet and the feed inlet are at opposite ends of the module. The feed and permeate flow rates are identical since the fiber operates in the dead-end mode.

To calculate the variations of pressure (p), flow velocity inside the fiber (v) and flux (J) as a function of the distance from the dead end of the fiber and the operating time, equations for local pressure, fluid velocity inside the fiber, and local flux are required. These equations can be driven from hydrodynamic relations in a hollow fiber membrane and membrane fouling models. Fig. 1 shows the pressures, flows, and dimensions in a fiber.

The local pressure inside a hollow fiber UF membrane can be described as Eq. (1) using the Hagen–Poiseuille equation, where no slip on the inside surface of the fiber is assumed. The pressure gradient along the x direction, dp/dx , is expressed as [3,8,9]:

$$\frac{dp(x,t)}{dx} = -\frac{32\eta v(x,t)}{D_i^2} \tag{1}$$

where p is the pressure, ρ is the density of water, v is the flow velocity inside the hollow fiber, η is the viscosity of water, D_i is the internal diameter of the fiber, and x is the distance from the dead-end of the fiber. The velocity gradient along the x direction is:

$$\frac{dv(x,t)}{dx} = \frac{4D_0J(x,t)}{D_i^2} \tag{2}$$

with the boundary conditions $v=0$ at $x=0$ and $v = (4D_0J_aL)/D_i^2$ at $x=L$ where J_a is the average flux

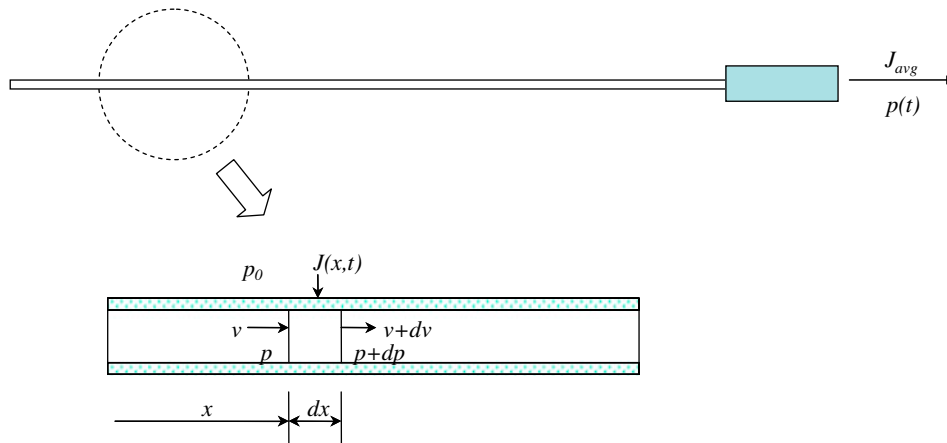


Fig. 1. Hydrodynamics inside a hollow fiber UF membrane.

over x . Then, the local TMP at time t is give as a function of the local flux:

$$p_0 - p(x, t) = \eta J(x, t) \left(R_m + \frac{\alpha m_d(x, t)}{A_m} \right) \quad (3)$$

where p_0 is the atmospheric pressure, R_m is the membrane resistance, α is the specific cake resistance, $\Delta P (=p_0 - p)$ is the applied pressure. For cake formed, the resistance can be described by:

$$\frac{\alpha}{A_m} \frac{dm_d(x, t)}{dt} = J(x, t)\alpha c = J(x, t)I \quad (4)$$

where c is the foulant concentration and $I(= \alpha c)$ is the fouling potential. In practice, the hollow fiber membrane was sealed with epoxy resin at its end, so the pressure at the $x=L$, $p|_{x=L}$, is slightly different from the pressure at the end of the fiber (p_t). Based on the

analytical solution of pressure drop in a nonporous tube, the pressure drop in the sealed part, Δp_{seal} , is given by Hwang et al. [3]:

$$p_t = p|_{x=L} + \Delta p_{\text{seal}} = p|_{x=L} + \frac{v|_{x=L}}{\sqrt{\frac{\rho D_0}{8\eta R_m} \tan h \left(\frac{4D_0 L_p}{D_i^2} \right)}} \quad (5)$$

where L_p is the sealed part length of the fiber.

Eqs. (1)–(3), were simultaneously solved using the initial and boundary conditions given by the operating conditions. For solving Eq. (3), it is necessary to calculate m_d , which can be given by Eq. (4). Moreover, the additional pressure drop by the potting region, which is described by Eq. (5), was used at the end of each calculation at a given time. Details are provided in our previous work [11]. The model was developed using Matlab as shown in Fig. 2.

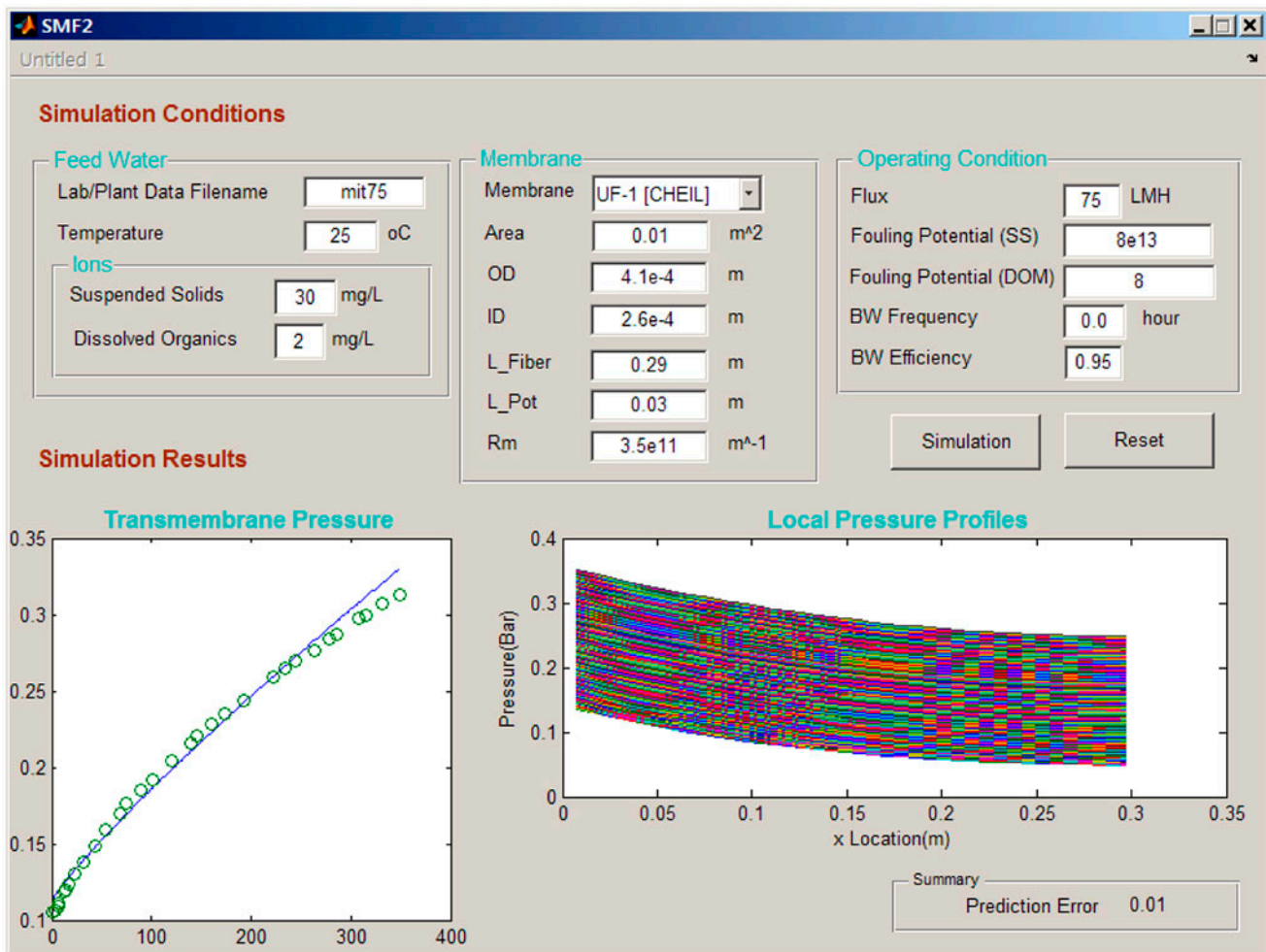


Fig. 2. A GUI of the Matlab model for UF simulation.

Table 1
Operating conditions of laboratory-scale submerged hollow fiber membrane test unit

Hollow fiber membrane characteristics		Experimental conditions	
Membrane materials	Polyvinylidene fluoride	Membrane module	Submerged, outside-in
Membrane surface area	0.01 m ²	Flux	50 L/m ² -h
OD/ID size	2.1/0.9 mm	Temperature	25 ± 0.5 °C
Fiber length	20 cm		

3. Experimental and method

3.1. Membrane filtration system

A schematic diagram of the submerged MF system used in this study is shown in Fig. 2. A tank having a working volume of 1 L was used for the filtration test of four hollow fiber membrane modules. Each module consisting of a single UF fiber was immersed and suspended vertically in the reactor. The UF fibers, made of polyvinylidene fluoride, were supplied by the Cheil Samsung Industry, Korea. They have a nominal pore size of 0.03 μm, an internal diameter of 0.9 mm and an

external diameter of 2.1 mm as shown in Table 1. The whole tests were carried out using the same membranes. Permeate from the membrane module was pulled by a peristaltic pump. The flux was frequently checked by collecting permeate on a mass cylinder and maintained constant throughout the operation by controlling the pump speed. The TMP were continuously measured by a pressure transducer (ISE40A-01-R, SMC, JAPAN) and a data logger (usb-6,008, NI, USA.) connected to a computer for data analysis. The temperature of solution was kept constant at 20 °C. Total recycle mode, where both the retentate from the UF loop and permeate were recycled into the tank, was adopted to keep the reactor volume constant during the operation time (see Fig. 3).

3.2. Procedure for UF tests

A mixture of water and blue indigo with a concentration of 20 mg/L was used as a feed. The Blue indigo (Sigma–Aldrich, 20 mg/L) has been used as a colored foulant in order to investigate the fouling pattern on the hollow fiber membrane. Each set of experiment started with four membrane modules. In every 2 h, one module was taken from the tank and dried for examination of membrane fouling, which could show the extent of fouling after 2, 4, 6, 8 h.

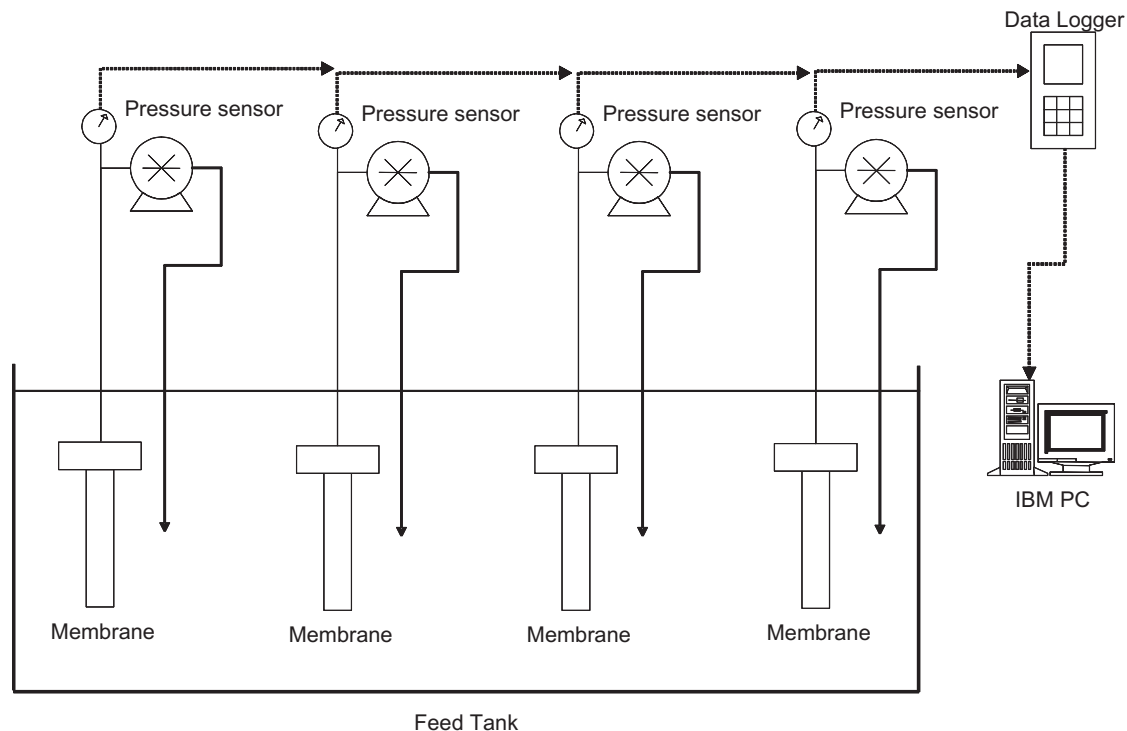


Fig. 3. Schematic diagram of experimental set-up for UF tests.

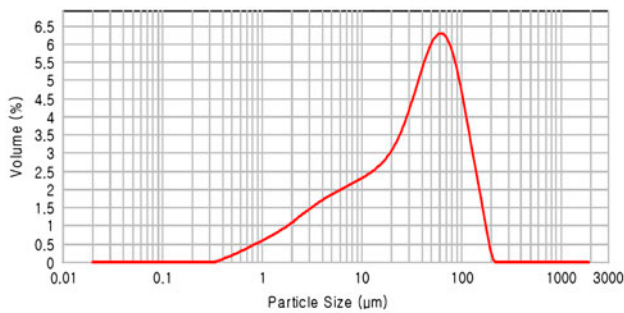


Fig. 4. Size distribution of blue indigo particles (Instrument: Malvern Mastersize 2000).

After each experiment, images of fouled membranes were captured by a digital camera and the images were analyzed. In these images, the blue color intensity represents the relative amount of foulants (blue Indigo) on the membrane surface. A quantitative analysis of the blue color covering pattern on the membrane sheet is carried out using Matlab. By importing the captured picture to this software it will be possible to find the color intensity of the dye along the membrane fiber. Using this software, the color images were converted to black and white images. Then, the relative number of black pixels were estimated and given as the concentration of foulants on the membrane surface.

4. Results and discussions

4.1. Filtration characteristics of UF fibers using blue indigo

Prior to the filtration tests, the characteristics of blue indigo particles were analyzed. Fig. 4 shows the

particle size distribution of the blue indigo. The volume weighted mean of the particle size was determined to 45.7 μm , although particles smaller than 1 μm also exist. As shown in Fig. 5, the zeta potential of the particles was -31.5 mV at 25 $^{\circ}\text{C}$. It was assumed that the size and zeta potential of the blue indigo are similar to those of the suspended solids in the surface water and seawater.

Fig. 6 shows TMP profiles for the UF test of the blue indigo particles [13]. At the beginning, four membranes were used using the same feed solution (blue indigo solution of 20 mg/L) and one was taken out for image analysis in every 2 h. After the test, the deposition of the blue indigo particles on the membrane fiber could be visually confirmed by examining the color. Nevertheless, the changes in the membrane permeability by the deposit formation were not substantial. The TMP ranged from 0.10 bar to 0.14 bar in most cases. Moreover, there was no significant increase in the TMP. The relative small increase in TMP by the blue indigo particle deposition can be attributed to the large particle size of blue indigo ($\sim 45 \mu\text{m}$). According to the filtration theory, large particles may not cause a significant increase in TMP.

The model was applied to fit the experimental data, as shown in Fig. 7. The increase in TMP by the blue Indigo solution was not significant. According to the model it, the I value was estimated to $4.2 \times 10^3 \text{ m}^2/\text{sec}$. Since the concentration of the blue Indigo was 20 mg/L, the α value was only $4.2 \times 10^3 \text{ m}^2/\text{kg}$. Again, the model fit confirms that the fouling rate is low. Using the model, the local pressure could be calculated, which are presented in Figs. 8 and 9. For instance, At 20 cm of

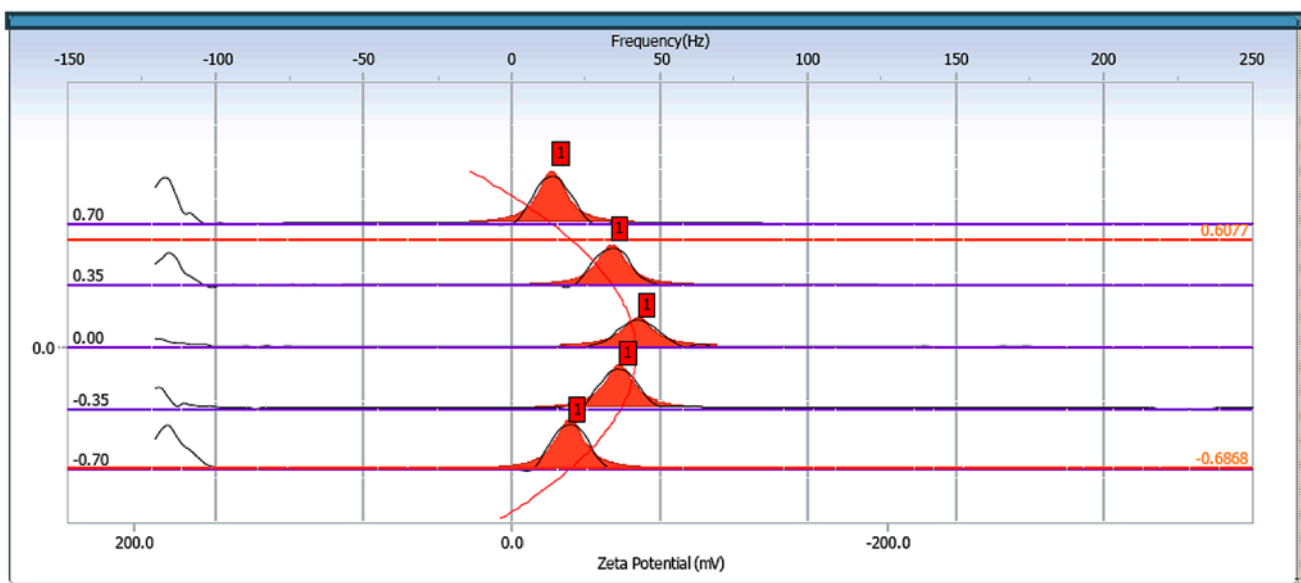


Fig. 5. Zeta potential of blue indigo particles (Instrument: Photal zeta meter).

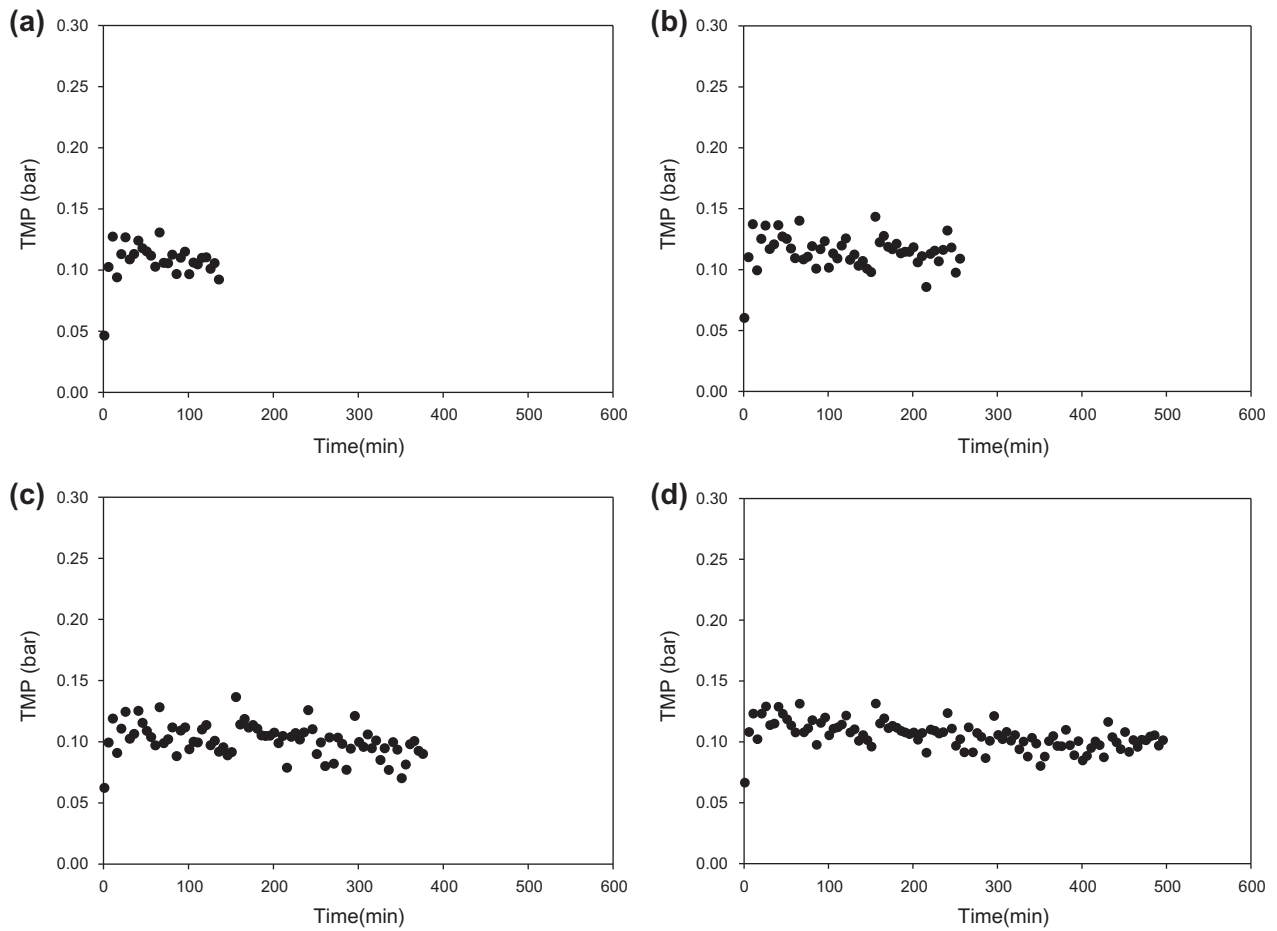


Fig. 6. Dependence of TMP on time for different membrane modules (a) No. 1 (b) No. 2 (c) No. 3 (d) No. 4.

distance from the fiber outlet, the local pressure and the local flux were about 10.9 kPa and 49.1 L/m²-h. Moreover, the local pressure and the local flux were about

11 kPa and 49.6 L/m²-h at the fiber outlet. Since the fiber inner diameter was relative large (0.9 mm) and the fiber length was short (20 cm), the difference in

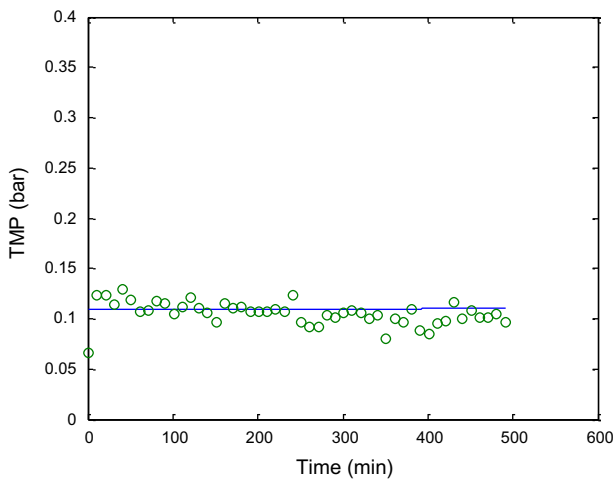


Fig. 7. Model fit to the experimental data for 8 h.

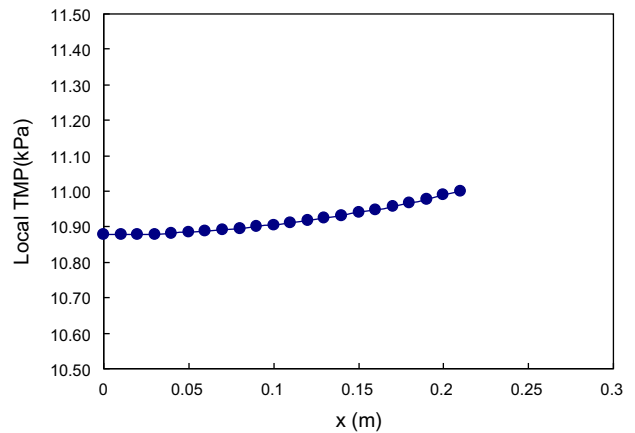


Fig. 8. Calculation of local pressure as a function of x position on a fiber.

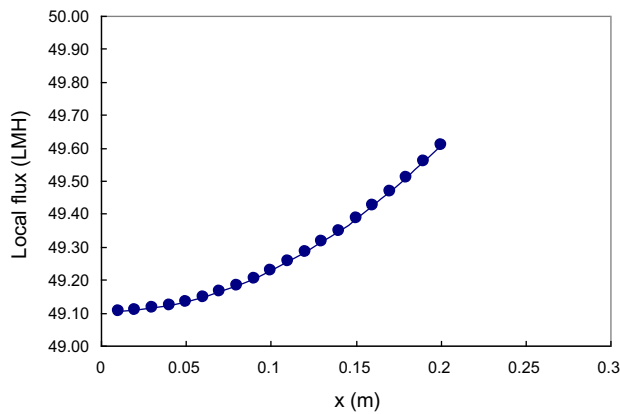


Fig. 9. Calculation of local flux as a function of x position on a fiber.

pressures and fluxes along the fiber was less than 2%. Nevertheless, the difference may be important if a longer fiber is used in the module. In full-scale modules, the fiber length is over 2 m, leading to a large difference between both ends of the fiber.

4.2. Deposition of blue indigo

Although blue indigo particles did not cause UF fouling in our tests, it appears that they formed deposits on the membrane surface. As shown in Fig. 10, the membrane was slightly covered by blue indigo after 2 h. The dark color on these pictures indicates that deposition of blue indigo. After 8 h, however, the membrane was almost completely covered. Clearly, the amount of deposits increased with filtration time.

It is likely that the surface coverage of the membrane is closely related to the amount of the deposits. Thus, an image analysis technique was applied to quantify the surface coverage. As shown in Fig. 11, the close-up image of the membrane surface was taken by a digital camera. Then the image was processed using the Matlab code to perform the thresholding. During the thresholding process, individual pixels in an image are marked as “object” pixels if their value is greater than some threshold value (assuming an object to be brighter than the background) and as “background” pixels otherwise. This

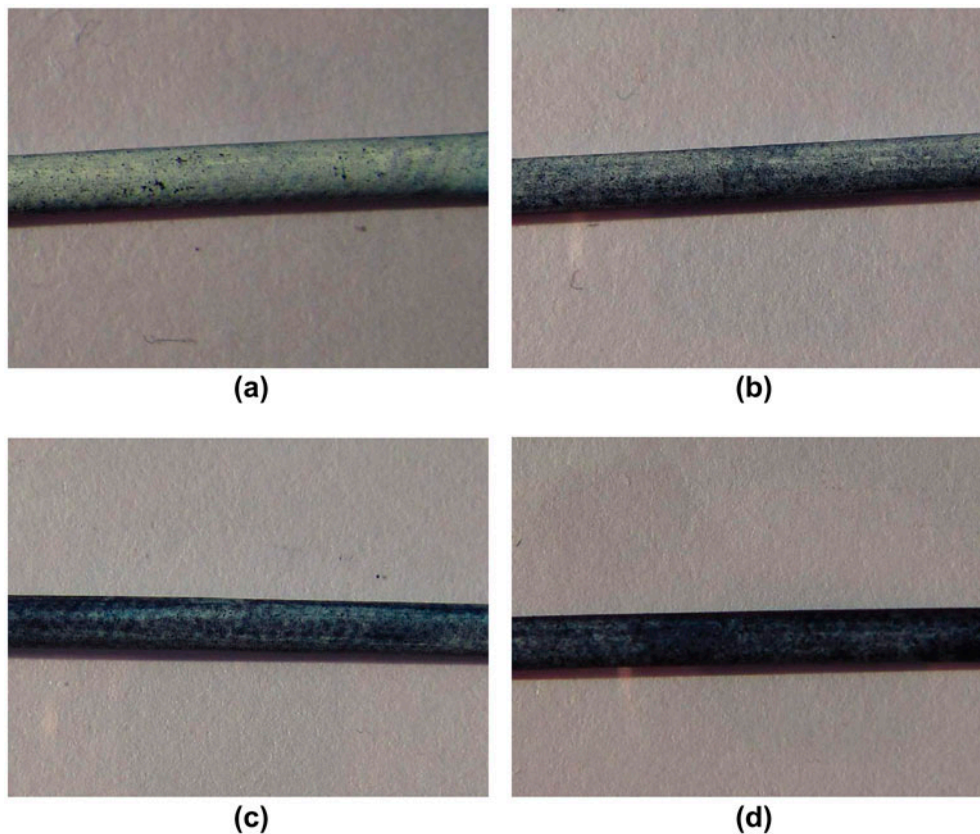


Fig. 10. Comparison of images for the membrane surface (position: outlet). (a) After 2 h (b) after 4 h (c) after 6 h (d) after 8 h.



Fig. 11. Image convert and threshold application (a) original image and (b) converted image for further analysis.

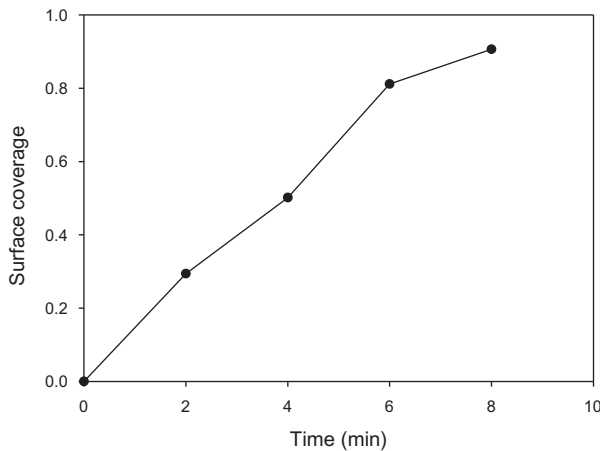


Fig. 12. Surface coverage as a function of filtration time in the outlet region.

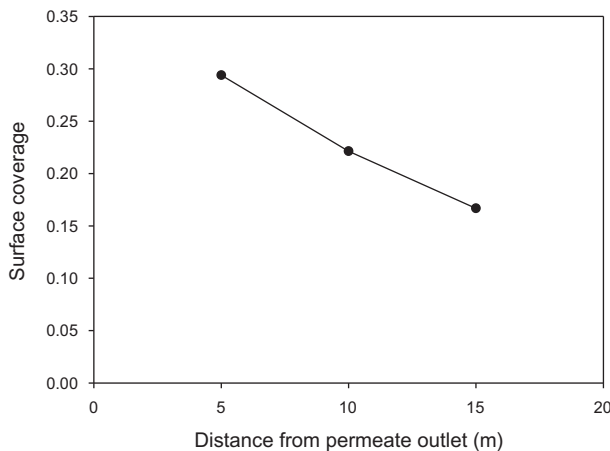


Fig. 13. Surface coverage as a function of distance from permeate outlet (after 2 h).

allows the calculation of the surface coverage. It should be noted that the accuracy of the image analysis depends on the threshold value. Using the trial-and-error approach, the optimum threshold value for the images were determined. The actual threshold value applied for this analysis was 60 (from 0 to 255).

Fig. 12 shows the surface coverage as a function of filtration time in the outlet region of the fiber. The results show that surface coverage is proportional to the filtration time. After 2 h, the surface coverage was 0.29 and increased up to 0.91 after 9 h. As described in Eq. (4), the deposited amount of foulants increases with time and local flux. Since fouling effect was negligible, the local flux was constant, leading to a linear relationship between foulant deposit and time. Although data is not shown, the surface coverage values in other regions (middle and dead end regions) show similar trends.

Fig. 13 shows the surface coverage as a function of location on the fiber at same time (after 2 h). The surface coverage was the highest (0.28) in the outlet region and the lowest in the dead end region (0.17). As illustrated in Fig. 7, the local flux is the highest in the outlet region and the lowest in the dead end region, which matches the results of the surface coverage analysis qualitatively. Nevertheless, there is a difference between the ratio of fluxes at both ends from the model calculation (1.02) and that of surface coverage from the image analysis (1.6). This suggests that not only the local flux but also other factors affect the deposition of blue indigo. The uneven stirring condition in the filtration tank could be the reason for these phenomena. Nevertheless, further works will be required for more quantitative analysis.

5. Conclusions

In this work, both theoretical and experimental methods were applied to analyze the filtration characteristics of submerged UF membrane. The model

applied here could provide invaluable information such as local pressure profiles and local fluxes. By fitting the model to the experimental data, fouling potential (I) and fouling constant (α) could be estimated. The experimental technique using blue indigo could visualize the local deposition of foulants, allowing the quantification of local foulant coverage through the image analysis techniques.

Accordingly, these methods are expected to be applied for quantitative analysis of foulant deposition on hollow fiber UF membrane. The model can be used for optimization of membrane modules under various situations. The visualization technique may be used for model verification for full-scale membrane modules. Of course, further works will be required to extend this approach for practical application fields such as water treatment and desalination in either pilot or full scale plants.

Acknowledgement

This research was supported by Korea Ministry of Environment as “The Eco-Innovation project (Global Top project)” (2012 001 080 003).

References

- [1] S. Chae, H. Yamamura, B. Choi, Y. Watanabe, Fouling characteristics of pressurized and submerged polyvinylidene fluoride (PVDF) microfiltration membranes in a pilot-scale drinking water treatment system under low and high turbidity conditions, *Desalination* 244 (2009) 215–226.
- [2] Y. Ye, L.N. Sim, B. Herulah, V. Chen, A.G. Fane, Effects of operating conditions on submerged hollow fiber membrane systems used as pre-treatment for seawater reverse osmosis, *J. Membr. Sci.* 365(1–2) (2010) 78–88.
- [3] K.J. Hwang, C.S. Chan, F.F. Chen, A comparison of hydrodynamic methods for mitigating particle fouling in submerged membrane filtration, *J. Chin. Inst. Chem. Eng.* 39 (2008) 257–264; M. Wdulf, C. Bartels, Optimization of seawater RO systems design, *Desalination* 173(1) (2005) 1–12.
- [4] G.D. Profio, X. Ji, E. Curcio, E. Drioli, Submerged hollow fiber ultrafiltration as seawater pretreatment in the logic of integrated membrane desalination systems, *Desalination* 269 (2011) 128–135.
- [5] Simon Atkinson, Research studies predict strong growth for MBR markets, *Membr. Technol.* 2 (2006) 8–10.
- [6] S. Chang, A.G. Fane, The effect of fiber diameter on filtration and flux distribution-relevance to submerged hollow-fiber modules, *J. Membr. Sci.* 184 (2001) 221–231.
- [7] K. Parameshwaran, C. Visvanathan, R.B. Aim, Membrane as solid/liquid separator and air diffuser in bioreactor, *J. Environ. Eng.* 125 (1999) 825–834.
- [8] J. Kim, F.A. DiGiano, Defining critical flux in submerged membranes: Influence of length-distributed flux, *J. Membr. Sci.* 280 (2006) 752–761.
- [9] S.-H. Yoon, H.-S. Kimb, I.-T. Yeomb, Optimization model of submerged hollow fiber membrane modules, *J. Membr. Sci.* 234 (2004) 147–156.
- [10] T. Carroll, N.A. Booker, Axial features in the fouling of hollow-fiber membranes, *J. Membr. Sci.* 168 (2000) 203–212.
- [11] S. Lee, P.-K. Park, J.-H. Kim, K.-M. Yeon, C.-H. Lee, Analysis of filtration characteristics in submerged microfiltration for drinking water treatment, *Water Res.* 42 (2008) 3109–3121.
- [12] C. Serra, M.J. Clifton, P. Moulin, J.-C. Rouch, P. Aptel, Dead-end ultrafiltration in hollow fiber modules: Module design and process simulation, *J. Membr. Sci.* 145 (1998) 159–172.
- [13] M. Rahimi, S.S. Madaeni, M. Abolhasani, Ammar Abdulaziz Alsairafi, CFD and experimental studies of fouling of a microfiltration membrane, *Chem. Eng. Process.: Process Intensification* 48 (2009) 1405–1413.